SETTING UP THE PRESERVATION OF FLUVIAL CHANNEL BELTS

Benjamin T. Cardenas[1,2]*, John M. Swartz[1,3,4,5], David Mohrig[1], and Eric W. Prokocki[1]

[1]University of Texas at Austin, Jackson School of Geosciences, Austin, TX, USA

[2]now at California Institute of Technology, Division of Geological and Planetary Sciences, Pasadena, CA, USA

[3]Institute for Geophysics, Jackson School of Geosciences, The University of Texas at Austin, Austin, TX, USA

[4]Department of Civil, Architectural, and Environmental Engineering, The University of Texas at Austin, Austin, TX, USA

[5]Department of Geosciences, Boise State University, Boise, ID, USA

*Corresponding author email: bencard@caltech.edu

ABSTRACT

Subsidence alone is often too slow to provide the necessary relief to preserve channel belts continuously over 10s of km, as is often observed in outcrop on Earth and Mars, as well as subsurface seismic volumes. A significant source of topographic relief was recently recognized along coastal plains of the US Gulf of Mexico and Atlantic, regions generally considered flat. Alluvial ridges, built from aggraded river-channel beds, bound topographically lower regions which develop tributary drainage networks initiating at the bounding ridges and draining seaward. This relief is capable of driving variability in fluvial sedimentation, thus controlling the way coastal river-channel belts accumulate and become preserved in the rock record. To show this, buried fluvial channel belts are mapped in a 3D seismic volume offshore of

the Brazos river delta, Texas, USA. Well-preserved fluvial channel belts are consistently mapped on top of surfaces possessing shorter channelized features. Horizons defined by short channelized features are interpreted as basal surfaces hosting the erosional channels of coastal tributary basins. The belts sitting above these surfaces record the occupation and filling of these basins following avulsions of major, sandy river systems. Both the focused sedimentation and the protection offered by the basin prevent the reworking of these belts, resulting in well-preserved belts recording 'strangely ordinary' transport conditions.

INTRODUCTION

External forcings, such as subsidence and sea-level change, are classically considered the primary controls on channel-belt preservation (Allen, 1978; Leeder, 1978; Bridge and Leeder, 1979; Wright and Marriott, 1993). Fluvial channel belts are, however, commonly preserved over km to 10s of km in locations where such continuous preservation is not expected due to low subsidence rates (Paola et al., 2018). At the bedform scale, topography larger than the bedform can drive relatively rapid sedimentation and can provide protection from later reworking, leading to well-preserved deposits (Reesink et al., 2015; Miall, 2015). For example, fully preserved fluvial dune "form-sets" are found at the downstream end of larger bar forms (Reesink et al., 2015). At larger scales, Paola et al. (2018) acknowledged the 'strange ordinariness' of much of the fluvial stratigraphic record, meaning these deposits represent apparently short durations at normal rather than extreme conditions. Is there a source of larger-scale topography capable of preserving fluvial channel-belts for km to 10s of km constructed under ordinary conditions, much as a bar helps to fully preserve a dune? Incised valleys fill this role (e.g., Alqahtani et al., 2015, 2017), but well-preserved channel belts are not limited to valley fills. Recently, drainage basins have been identified across the coastal plains of the US Gulf of Mexico and Atlantic Ocean (Willett et al., 2014; Swartz et al., in review). These basins provide up to 10s of m of relief for the potential preservation of channel-belt segments 10s of km in length (Fig. 1; Swartz et al., in review). Raised alluvial ridges, constructed by active coastal rivers, make up the drainage divides between these tributary basins (Fig. 1). Smaller-scale erosional tributary channel networks drain water and sediment from tributary basins into the gulf, thus limiting floodplain aggradation and creating additional erosional relief (Fig. 1; Swartz et al., in prep).

We hypothesize that the larger-scale primary depositional channels could avulse and re-route into adjacent tributary basins, where they could fill topographic levels below the reworking depths of primary fluvial activity. This hypothesis is tested by 3D seismic reflection volume mapping of fluvial channel belts preserved in the subsurface Gulf of Mexico offshore Brazos River, TX, USA. 3D seismic reflection volumes have been proven useful in reconstructing the kinematics of ancient fluvial systems (Miall, 2002; Wood, 2007; Hubbard et al., 2011; Armstrong et al., 2014; Jobe et al., 2016; Alqahtani et al., 2017; Martin et al., 2018: Zeng, 2018), and towards understanding preservation and re-working within channel belts (Durkin et al., 2018). In this study, the term “channel belt” defines the sum total of all channel-filling deposits left by a river, regardless of how much, or how little, lateral migration and aggradation was recorded (Blum and Törnqvist, 2000; Gibling, 2006; Jerolmack and Mohrig, 2007). We do not define a channelized feature lacking channel fill as a channel belt.

METHODS

A 3D seismic reflection volume of the Brazos River delta was downloaded from the National Archive of Marine Seismic Surveys (NAMSS; volume B-18-93-TX). This data volume was collected in 1993 and covered an area of ~2,300 km^2 from 15 km to 50 km offshore Texas (Fig. 2), with lines spaced 20 m apart. This study was restricted to the relatively shallow subsurface, the first 1000 milliseconds of acoustic wave two-way-travel time (ms TWT), with 0 at sea level and values becoming more negative with increasing depth. This volume clearly imaged four clusters of channelized features with the best possible resolution afforded by the highest possible frequency content for the reflected acoustic waves. Amplitude volumes from the NAMSS were opened in Petrel software to map the bottom surfaces of channelized features in cross-sectional views (Fig. 3A-E). The amplitude volumes were then processed into variance volumes, which placed strong returns where adjacent seismic lines were less similar, and weak returns where adjacent lines are more similar (Bahorich and Farmer, 1995). This can be considered a 3D volume of amplitude curvature, or edge detection, which has been demonstrated to accentuate channel-belt boundaries (Bahorich and Farmer, 1995; Liu and Marfurt, 2007; Armstrong, 2012). Furthermore, time slices from the variance volume were used to map channelized features and to define underlying surfaces interpreted as defining tributary basins. Ultimately these basal surfaces were mapped in the amplitude volume that provided the greatest vertical resolution (Fig. 3A-E). The basal surfaces of channelized features were mapped across the feature's lateral extent as observed in the time slice variance image, using truncated reflectors as a guide (Fig. 3B-C). Surfaces mapped in the along-belt direction (Fig. 3D-E) were then used to tie cross sections (Fig. 3B) to less obvious views (Fig. 3C). Next, surfaces interpolated between mapped horizons were converted to grids of points with XYZ coordinates, where a distribution of Z values (depth in units of ms TWT) was extracted from each surface to help quantify its stratigraphic position.

After cross-sectional mapping, selected variance time slices were exported from Petrel and into ArcGIS, in order to perform more robust planview mapping operations (Alqahtini et al., 2017). The centerline length and average width of channel belts were calculated by first mapping the opposite long edges of each feature as a series of ~2 m spaced points with XY coordinates. A local measurement of width was made from each point along one edge to the nearest point on the opposite edge using an automated script, and a centerline point was placed halfway between the two points. Width measurements were averaged for each feature, and the centerline length was calculated as the sum of the distances between successive centerline points.

RESULTS

Two populations of channelized features were identified in each of the four survey zones (Fig. 2). The division between populations is clear upon visual inspection (Figs. 4A-L) and quantification (Table 1; Fig. 5A). Of the 156 mapped channelized features, 17 define a population of longer features, and the remaining 139 define a population of shorter features (Table 1). To test if the shorter channelized features define the bottom of an eroded tributary drainage basin filled by the longer channelized features, we observed the stratigraphic arrangement of long and short features using time slices at different depths (Fig. 4), histograms of ms TWT values (Fig. 5), 3-D renderings (Fig. 6), and depth profiles (Fig.7). The 3-D renderings, depth profiles, and histograms both compare a "zone-scale basal surface" to the longer channelized features. The zone-scale basal surfaces were created in Petrel by interpolating a 3-D surface between the mapped bases of the shorter channelized features, limited to each zone's extent (Fig. 1). There is a consistent stratigraphic arrangement of the long channelized features and the zone-scale basal surfaces in zones 1-3, with the shorter channelized features from 0 to 60 ms TWT beneath the longer channelized features (Figs. 4-7). There is no instance of a group of longer channelized features located beneath shorter features. Zone 4 also contains both types of channelized feature in a similar arrangement, but both exist within a larger topographic container not observed in zones 1-3 (Figs. 5 and 8). Rather, zone 4's basal surface is instead defined by a larger-scale topographic container, which has a distinct distribution of depth values, including a range 3 times larger than the other zones (~300 ms TWT vs. 60-100 ms TWT; Fig. 5E) and a long tail towards shallower depths (Fig. 5E). In variance time slices, this surface has a scalloped shape and acts as a western boundary to the zone 4 channel-belt cluster (Fig. 4).

DISCUSSION

The two populations of channelized features, distinguished by length (Fig. 5A; Table 1), record the kinematics and filling of their formative river channels (Gibling, 2006; Jerolmack and Mohrig, 2007). The longer features are interpreted as narrow channel belts. They are mappable for km because they have not been reworked following their deposition, and because they maintain an impedance contrast with the surrounding sediment, likely due to a consistent sandy channel fill relative to adjacent muds. The shorter features lack this continuous impedance contrast (Fig. 4; Table 1), and thus are not interpreted as channel belts, but as erosional channels later filled by muds. The time slices (Fig. 4A-F), depth histograms (Figs. 5B-E), 3-D renderings (Fig. 6), and show that the zone-scale basal surfaces defined by the short erosional channels sit just 0-60 ms TWT below the long channel belts, or are slightly scoured by them. This arrangement is shown particularly clearly in the zone 2 depth profiles shown in Figure 7, and highlights the fact that this relationship is held across the entire length of a channel belt (Fig. 7C). These basal surfaces are interpreted to be the stratigraphic representations of a network of these erosional, mud-filled channels. The stratigraphic arrangement of these two sedimentologically contrasting deposits, with an erosional surface containing well-preserved channel belts, is consistent with the filling of erosional tributary drainages by avulsive, sandy rivers and associated overbank muds.

Hajek and Heller (2012) demonstrated that changes in the ratio of flow depth vs. floodplain aggradation rates can change the degree of channel-belt preservation observed through time, where their numerical modeling and field example (the Castlegate Sandstone, Utah, USA) represent examples showing how the dominant control is change in flow depth, with steady accumulation rates. However, in this study, the apparent dependence of well-preserved belts on nearby (0-60 ms TWT) reworked surfaces instead favors a rapid change in local sedimentation rates triggered by sudden basin infilling. This preservation mechanism is largely independent of basin subsidence. Paola et al. (2018) recognized the discrepancy between channel belt preservation and subsidence rate in the Mississippi River delta. Belts from 4 to 30 km in length are preserved, even though the time required to create that space through subsidence is 10-

50 times reasonable avulsion periods. Coastal tributary basins provide the relief necessary to preserve these belts, and provide a potential answer to one of the major questions asked by Paola et al. (2018): "What physical processes modulate local rates of deposition so as to produce high rates of deposition without high transport rates, leading to extraordinary preservation of ordinary events?" While it has been demonstrated that hierarchical topography can drive this variability in sedimentation at the bedform scale (Reesink et al., 2015; Cardenas et al., 2019), it is evidenced in this study to also be acting at the channel-belt scale. This is also significant in that a local topographic control was the immediate forcing upon these coastal fluvial systems, rather than a global control (i.e., relative sea level, subsidence). Deposition within these basins provides for local variability in basin-averaged sedimentation rates, a concept noted by Sadler and Jerolmack (2015).

Zone 4 is interpreted as a package of channel belts filling an incised valley based on the scalloped wall geometry (Fig. 4K-L) associated with truncated reflectors (Fig. 8), consistent with formation by outer-bank erosion by migrating rivers (e.g., Zaitlin et al., 1994; Armstrong, 2012; Cardenas et al., 2018) and the overall package thickness (Fig. 5E). The preservation of channel belts over several km within this valley is consistent with the demonstrated significance of hierarchical topography when setting up the preservation of fluvial channel belts. Although zones 1-3 make clear that an incised valley is not the only possible source of such topography, zone 4 provides an interesting contrast where the construction of the containing topography is controlled by external forcings (i.e., valley cutting and filling associated with relative sea-level change, Simms et al., 2007). In Figures 4K-L, poorly preserved belts are also observed within the valley, suggesting the possible development of coastal tributary basins within even larger-scale valleys.

CONCLUSIONS

The development and filling of coastal tributary basins, which are common geomorphic features across the modern US Gulf of Mexico coast, leaves well-preserved fluvial channel belts in the stratigraphic record of the Gulf of Mexico without the requirement of an incised valley, and significantly, in the absence of subsidence rates high enough to create channel-belt-scale relief on avulsion timescales (Paola et al., 2018). The development of these basins may also be an important control on channel-belt clustering (Hajek et al., 2010). We posit that, because such preservation has been observed in other parts of the world beyond the extent of incised valleys (e.g., Miall, 2002; Martin et al., 2018), these basins may have commonly helped preserve channel belts across Earth by acting as a higher hierarchical source of topography, leading to the 'strange ordinariness' of much of the fluvial stratigraphic record (Paola et al., 2018). Well-preserved channel belts exhumed on Earth (Hayden et al., 2019; Cardenas et al., in review) and the surface of Mars (Burr et al., 2009; DiBiase et al., 2013; Kite et al., 2015; Davis et al., 2016; Cardenas et al., 2018; Hughes et al., 2019) may also represent the construction of these basins. Further work should investigate the consistency of the results presented here across the Gulf of Mexico, along other coasts both similar and dissimilar to the Gulf of Mexico in terms of dominant processes, and other alluvial systems where these tributary basins may develop between channels, such as foreland basin megafans/distributive fluvial systems (Horton and DeCelles, 2001; Weissman et al., 2013; Owen et al., 2015). Additionally, the lengths of channel belts can be further developed as a constraint on the kinematics and filling of ancient channels, especially in seismic volumes or remote sensing datasets where belt thickness, an important recorded of channel kinematics (Gibling, 2006; Jerolmack and Mohrig, 2007) cannot be well constrained.

ACKNOWLEDGEMENTS

BTC thanks Zoltan Sylvester and Joel Johnson for helpful reviews of this manuscript, and Mike Lamb for helpful discussions. We thank the United States Geologic Survey for maintaining the National Archive of Marine Seismic Surveys at http://walrus.wr.usgs.gov/namss/. BTC acknowledges funding from the The University of Texas at Austin Graduate School, the Jackson School of Geosciences, and the RioMAR Industry Consortium.

REFERENCES

Allen, J.R.L., 1978, Studies in fluviatile sedimentation: an exploratory quantitative model for the architecture of avulsion-controlled alluvial suites: Sedimentary Geology, v. 21, p. 129-147.

Alqahtani, F.A., Johnson, H.D., Jackson, C.A.-L., and Som, M.R.B., 2015, Nature, origin and evolution of a Late Pleistocene incised valley-fill, Sunda Shelf, Southeast Asia: Sedimentology, v. 62, p. 1198-1232.

Alqahtani, F.A., Jackson, C.A.-L., Johnson, H.D., and Som. M.R.B., 2017, Controls on the geometry and evolution of humid-tropical fluvial systems: Insights from 3D seismic geomorphological analysis of the Malay Basin, Sunda Shelf, Southeast Asia: Journal of Sedimentary Research, v. 87, p. 17-40.

Armstrong, C., 2012, 3D seismic geomorphology and stratigraphy of the Late Miocene to Pliocene Mississippi River delta: fluvial systems and dynamics: Master's Thesis, University of Texas at Austin, Austin, TX, 119 p.

Armstrong, C., Mohrig, D., Hess, T., George, T., and Straug, K.M., 2014, Influence of growth faults on coastal fluvial systems: examples from the late Miocene to recent Mississippi River Delta: Sedimentary Geology, v. 301, p. 120-132.

Bahorich, M., and Farmer, S., 1995, 3-D seismic discontinuity for faults and stratigraphic features: The coherence cube: The Leading Edge, v. 14, p. 1021-1098.

Blum, M.D., and Törnqvist, T.E., 2005, Fluvial responses to climate and sea-level change: a review and look forward: Sedimentology, v. 47, p. 2-48.

Bridge, J.S., and Leeder, M.R., 1979, A simulation model of alluvial stratigraphy: Sedimentology, v. 26, p. 617-644.

Burr, D.M., Enga, M.-T., Williams, R.M.E., Zimbelman, J.R., Howard, A.D., and Brennand, T.A., 2009, Pervasive aqueous paleoflow features in the Aeolis/Zephyria Plana region, Mars: Icarus, v. 200, p. 52-76.

Cardenas, B.T., Kocurek, G., Mohrig, D., Swanson, T., Hughes, C.M., and Brothers, S.C., 2019, Preservation of autogenic processes and allogenic forcings within set-scale aeolian architecture II: the scour-and-fill dominated Jurassic Page Sandstone, Arizona, USA: Journal of Sedimentary Research, v. 89, p. 741-760.

Cardenas, B.T., Mohrig, D., and Goudge, T.A., 2018, Fluvial stratigraphy of valley fills at Aeolis Dorsa, Mars: Evidence for base-level fluctuations controlled by a downstream water body: Geological Society of America Bulletin, v. 130, p. 484-498.

Cardenas, B.T., Mohrig, D., Hughes, C.M., Goudge, T.A., Levy, J.S., Swanson, T., Mason, J., and Zhao, F., in review, The anatomy of exhumed river-channel belts. Pre-print available at EarthArxiv: https://eartharxiv.org/zw4hr/

Chamberlin, E.P., and Hajek, E.A., 2019, Using bar preservation to constrain reworking in channel-dominated fluvial stratigraphy: Geology, v. 47, p. 531-534.

Davis, J.M., Balme, M., Grindrod, P.M., Williams, R.M.E., and Gupta, S., 2016, Extensive Noachian fluvial systems in Arabia Terra: Implications for early Martian climate: Geology, v. 44, p. 847-850.

DiBiase, R.A., Limaye, A.B., Scheingross, J.S., Fischer, W.W., and Lamb, M.P., 2013, Deltaic deposits at Aeolis Dorsa: Sedimentary evidence for a standing body of water on the northern plain of Mars: Journal of Geophysical Research: Planets, v. 118, p. 1285-1302.

Durkin, P.R., Hubbard, S.M., Holbrook, J., and Boyd, R., 2018, Evolution of fluvial meander-belt deposits and implications for the completeness of the stratigraphic record: Geological Society of America Bulletin, v. 130, p. 721-739.

Gibling, M.R., 2006, Width and thickness of fluvial channel bodies and valley fills in the geologic record: a literate compilation and classification: Journal of Sedimentary Research, v. 76, p. 731-770.

Hajek, E.A., Heller, P.L., and Sheets, B.A., 2010, Significance of channel-belt clustering in alluvial basins: Geology, v. 38, p. 535-538.

Hajek, E.A., and Heller, P.L., 2012, Flow-depth scaling in alluvial architecture and nonmarine sequence stratigraphy: example from the Castlegate Sandstone, Central Utah, U.S.A.: Journal of Sedimentary Research, v. 82, p. 121-130.

Hayden, A.T., Lamb, M.P., Fischer, W.W., Ewing, R.C., McElroy, B.J., and Williams, R.M.E., 2019, Formation of sinuous ridges by inversion of river-channel belts in Utah, USA, with implications for Mars: Icarus, in press.

Hubbard, S.M., Smith, D.G., Nielsen, H., Leckie, D.A., Fustic, M., Spencer, R.J., and Bloom, L., 2011, Seismic geomorphology and sedimentology of a tidally influenced river deposit, Lower Cretaceous Athabasca oil sands, Alberta, Canada: American Association of Petroleum Geologists Bullet, v. 95, p. 1123-1145.

Hughes, C.M., Cardenas. B.T., Goudge, T.A., and Mohrig, D., 2019, Deltaic deposits indicative of a paleo-coastline at Aeolis Dorsa, Mars: Icarus, v. 317, p. 442-453.

Jerolmack, D.J., and Mohrig, D., 2007, Conditions for branching in depositional rivers: Geology, v. 35, p. 463-466.

Jobe, Z.R., Howes, N.C., and Auchter, N.C., 2016, Comparing submarine and fluvial channel kinematics: Implications for stratigraphic architecture: Geology, v. 44, p. 931-934.

Kite, E.S., Howard, A.D., Lucas, A.S., Armstrong, J.C., Aharonson, O., and Lamb, M.P., 2015, Stratigraphy of Aeolis Dorsa, Mars: Stratigraphic context of the great river deposits: Icarus, v. 253, p. 223-242.

Leeder, M.R., 1978, A quantitative stratigraphic model for alluvium, with special reference to channel deposit density and interconnectedness: Canadian Society of Petroleum Geologists Memoir 5, p. 587-596.

Liu, J., and Marfurt, K.J., 2007, Instantaneous spectral attributes to detect channels: Geophysics, v. 72, p. 23-31.

Martin, J., Fernandes, A.M., Pickering, J., Howes, N., Mann, S., and McNeil, K., 2018, The stratigraphically preserved signature of persistent backwater dynamics in a large paleodelta system: The Mungaroo Formation, North West Shelf, Australia: Journal of Sedimentary Research, v. 88, p. 850-872.

Miall, A.D., 2002, Architecture and sequence stratigraphy of Pleistocene fluvial systems in the Malay basin, based on seismic time-slice analysis: American Association of Petroleum Geologists Bulletin, v. 86, p. 1201-1216.

Miall, A.D., 2015, Updating uniformitarianism: stratigraphy as just a set of ‘frozen accidents’: Geological Society, London, Special Publications, v. 404, p. 11-36.

Owen, A., Nichols, G.J., Hartley, A.J., Weissmann, G.S., and Scuderi, L.A., 2015, Quantification of a distributive fluvial system: The Salt Wash DFS of the Morrison Formation, SW U.S.A.: Journal of Sedimentary Research, v. 85, p. 544-561.

Paola, C., Ganti, V., Mohrig, D., Runkel, A.C., and Straub, K.M., 2018, Time not our time: physical controls on the preservation and measurement of geologic time: Annual Review of Earth and Planetary Sciences, v. 46, p. 409-438.

Reesink, A.J.H., Van den Berg, J.H., Parsons, D.R., Amsler, M.L., Best, J.L., Hardy, R.J., Orfeo, O., Szupiany, R.N., 2015, Extremes in dune preservation: Controls on the completeness of fluvial deposits: Earth-Science Reviews, v. 150, p. 652-665.

Sadler, P.M., and Jerolmack, D.J., 2015, Scaling laws for aggradation, denudation and progradation rates: the case for time-scale invariance at sediment sources and sinks: Geological Society, London, Special Publications, v. 404, p. 69-88.

Simms, A.R., Anderson, J.B., Milliken, K.T., Taha, Z.P., and Wellner, J.S., 2007, Geomorphology and age of the Oxygen isotope stage 2 (last lowstand) sequence boundary on the northwestern Gulf of Mexico continental shelf: Geological Society, London, Special Publications, v. 277, p. 29-46.

Swanson, T., Mohrig, D., Kocurek, G., Cardenas, B.T, and Wolinsky, M.A., 2019, Preservation of autogenic processes and allogenic forcings within set-scale aeolian architecture I: numerical experiments: Journal of Sedimentary Research, accepted.

Swartz, J.M., Cardenas, B.T., Mohrig, D., and Passalacqua, P., in review for the same issue, From distributary to tributary: Formation of channel networks set by depositional processes.

Weissman, G.S., Hartley, A.J., Scuderi, L.A., Nichols, G.J., Davidson, S.K., Owen, A., Atchley, S.C., Bhattacharyya, P., Chakraborty, T., Ghosh, P., Nordt, L.C., Michel, L., and Tabor, N.J. (2013)

Prograding distributive fluvial systems – Geomorphic models and ancient examples. in SEPM Special Publication 2014, New Frontiers in Paleopedology and Terrestrial Paleoclimatology, 131-147.

Willett, S.D., McCoy, S.W., Perron, J.T., Goren, L., and Chen, C.-Y., 2014, Dynamic reorganization of river basins: Science, v. 343, no. 1248765.

Wood, L.J., 2007, Quantitative seismic geomorphology of Pliocene and Miocene fluvial systems in the northern Gulf of Mexico, U.S.A.: Journal of Sedimentary Research, v. 77, p. 713-730.

Wright, V.P., and Marriott, S.B., 1993, The sequence stratigraphy of fluvial depositional systems: The role of floodplain sediment storage: Sedimentary Geology, v. 86, p. 2013-210.

Zaitlin, B.A., Dalrymple, R.W., and Boyd, R., 1994, The stratigraphic organization of incised-valley systems associated with relative sea-level change: in Dalrymple, R.W., Boyd, R., and Zaitlin, B.A., eds., Incised-Valley Systems: Origin and Sedimentary Sequences: SEPM, Special Publication 51, p. 45-60.

Zeng, H., 2018, What is seismic sedimentology? A tutorial: Interpretation, v. 6, SD1-SD12.

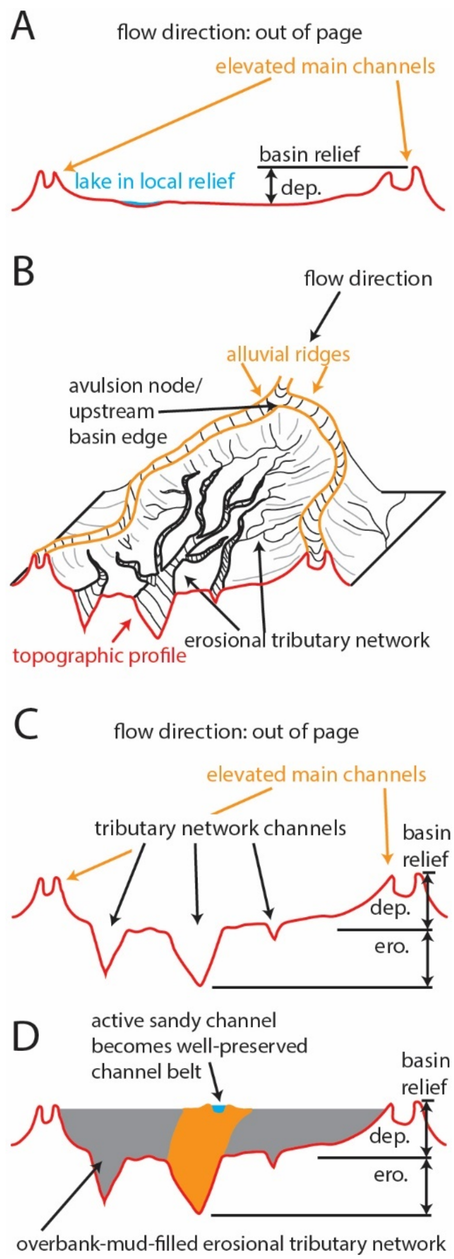

Figure 1 (5.9 cm X 13.4 cm) – A: Schematic transect between two raised alluvial ridges without the development of an erosional tributary network. Relief only forms from the decrease in sedimentation away from the main channels. While some local relief can create lakes. the overall relief is less than in panels B and C. B: Three-dimensional illustration of an erosional tributary network developed within a basin confined and bounded by alluvial ridges (Swartz et al., in review). Alluvial ridges built by larger, sand-transporting channels (orange) define the basin boundaries. The erosional tributary network is drawn using black lines. The topographic profile at the edge of the diagram is shown with the red line, with the erosional channels generating v-shaped incisions. C: The red line showing relief in panels A and B. This relief is generated due to decreased sedimentation away from the channel (A), as well as the erosional tributary network channels (B). D: A sandy depositional channel has avulsed into the basin, where it has filled the basin with a sandy channel belt and muddy overbank deposits.

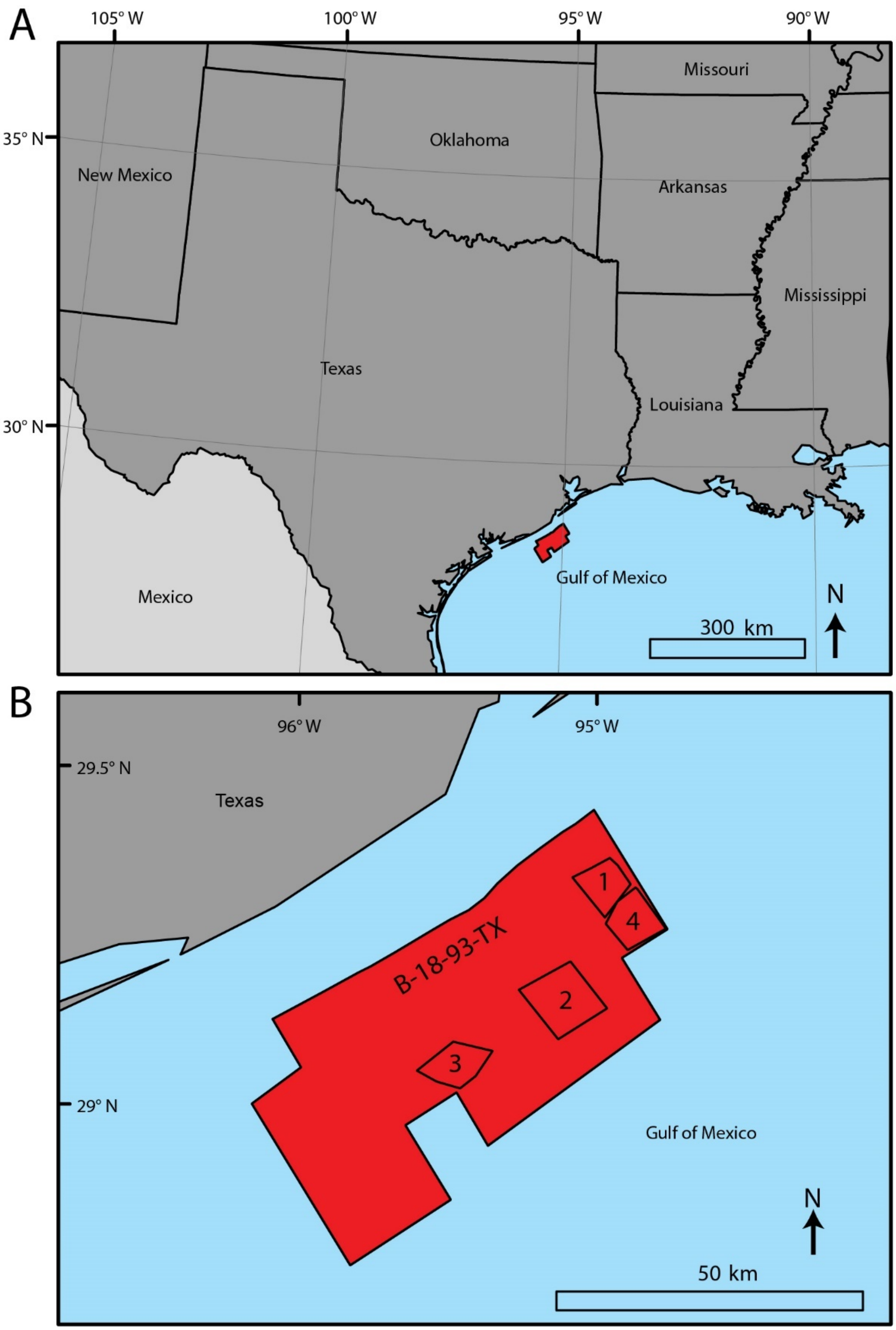

Figure 2 – A: Location map for the offshore seismic survey B-18-93-TX. The spatial extent of the survey is mapped in red. B: Zoom in to the survey area, with the mapped extent of the four studied zones.

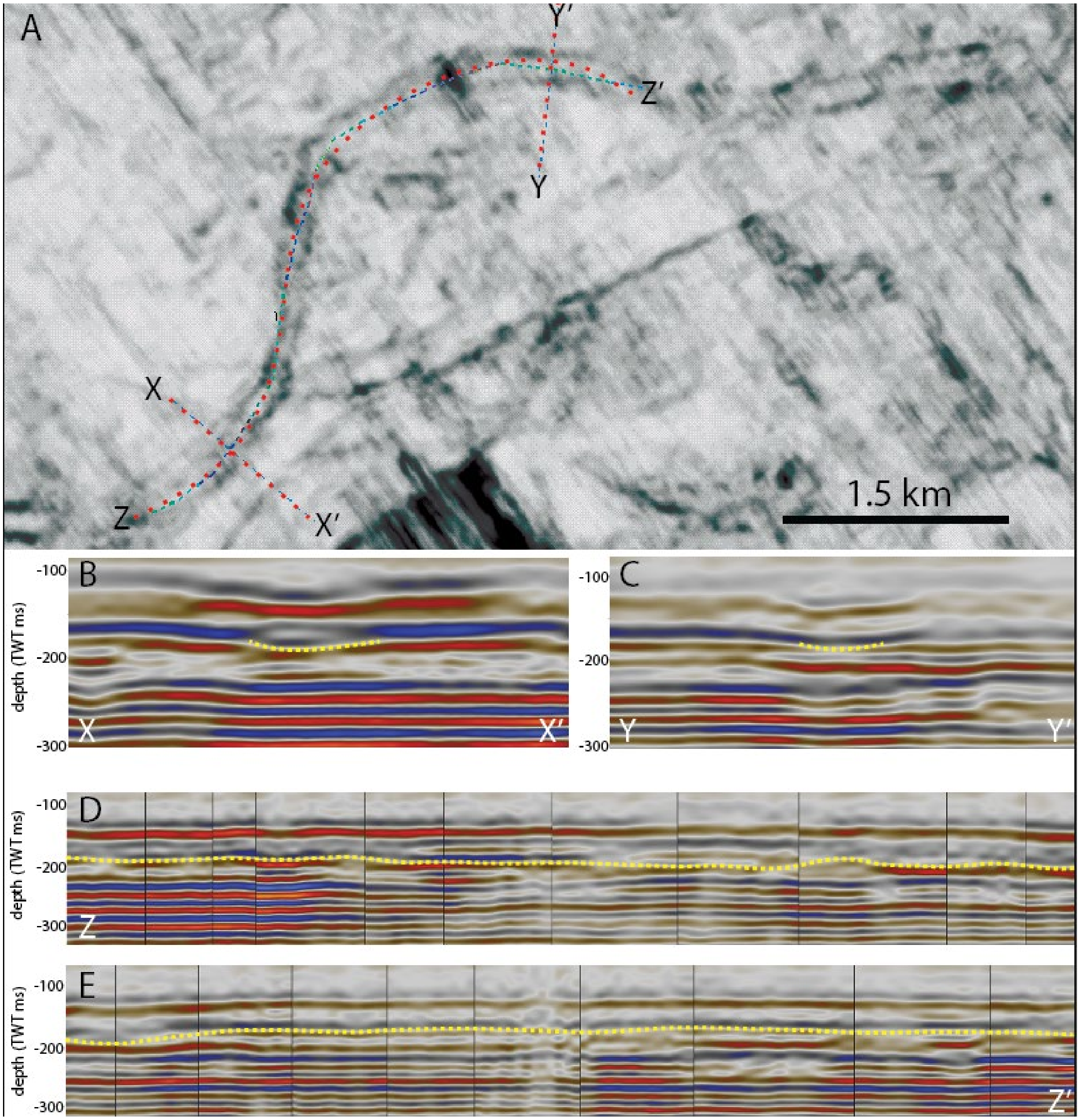

Figure 3 (18.5 cm x 19.2 cm) – A: Variance time slice showing a fluvial channel belt from zone 2 (Fig. 2). Lines X-X′ and Y-Y′ show the locations of cross-belt sections in panels B and C. Line Z-Z′ defines an approximate centerline section for the belt that is presented in panels D and E. B: Cross-section X-X′, with a yellow line marking the belt base. Erosion by this surface clearly truncated reflectors to either side of the channel belt. C: Cross-section Y-Y′ with a yellow line marking the interpreted base of the same belt.

The amplitude contrast at the belt base is not as stark as in X-X’. D and E: Cross-section Z-Z’ over two panels. The belt bottom mapped in this cross-section ties X-X’, where the belt is clearly identified, to Y-Y’, where it is less easily identified.

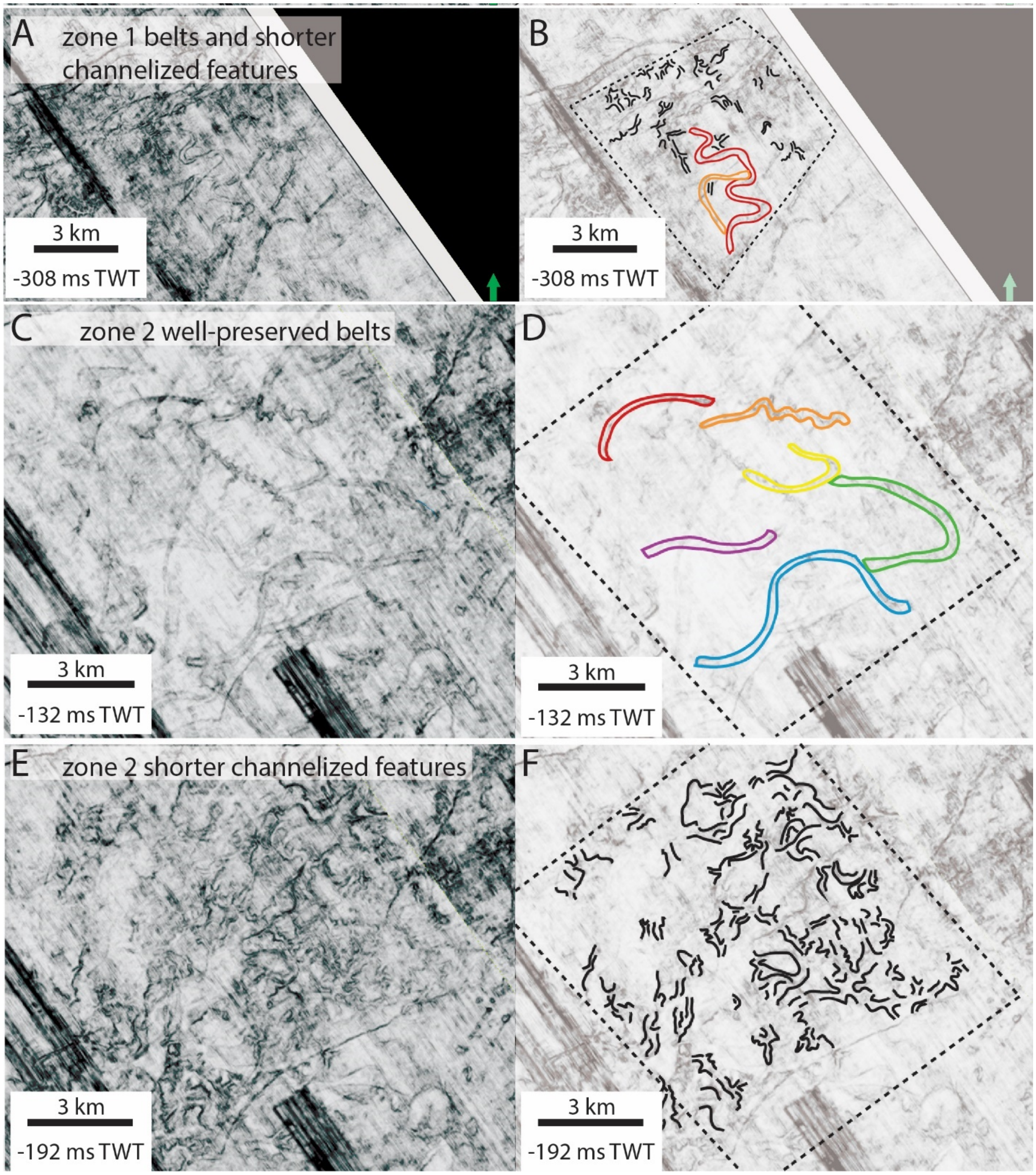

A
zone 1 belts and shorter channelized features
3 km
-308 ms TWT
B
3 km
-308 ms TWT
C
zone 2 well-preserved belts
3 km
-132 ms TWT
D
3 km
-132 ms TWT
E
zone 2 shorter channelized features
3 km
-192 ms TWT
F
3 km
-192 ms TWT

337

338

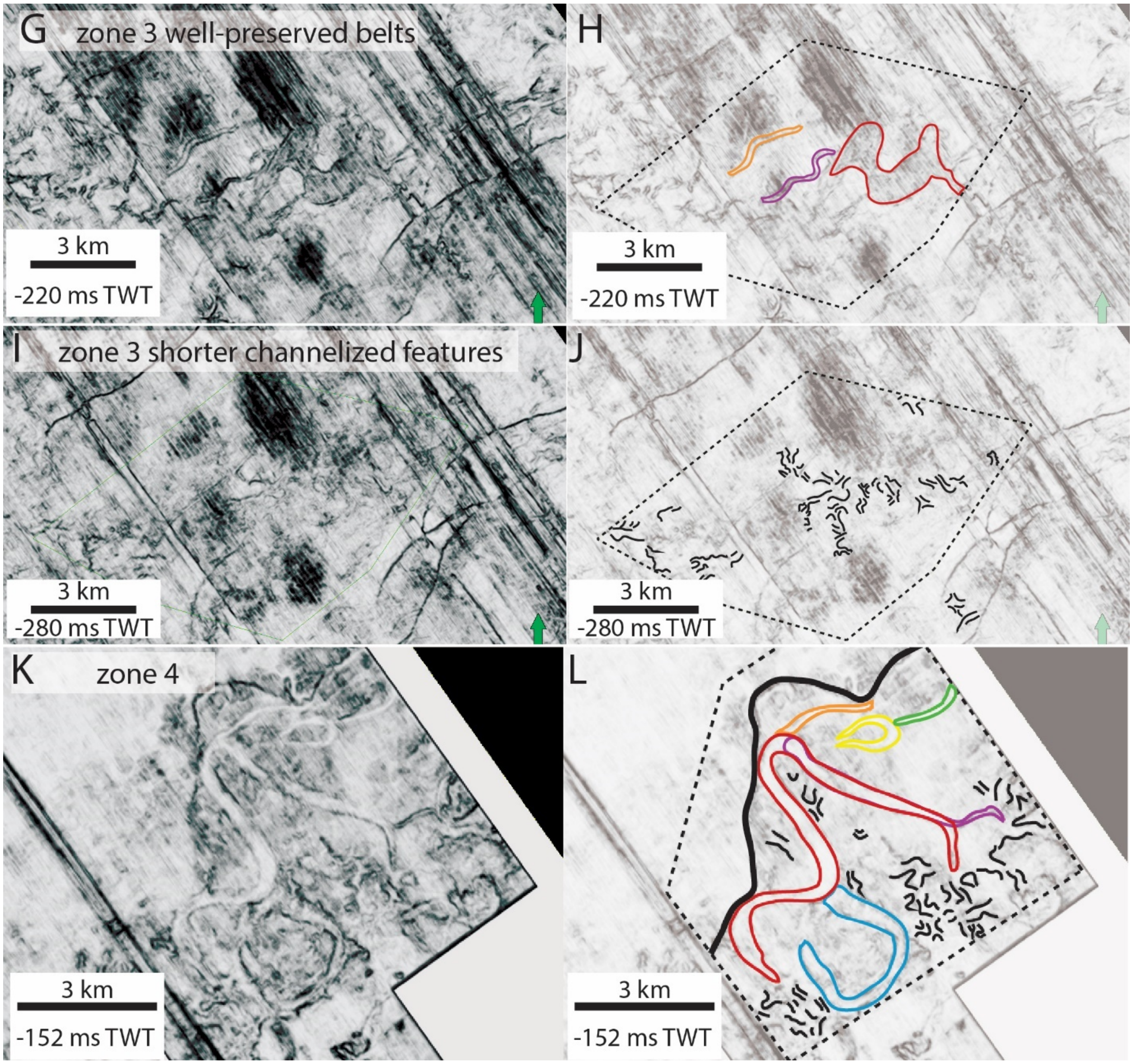

339 Figure 4 – Time slices from the variance volume showing long channelized features (colored lines), short
340 channelized features (black lines), and the mapped extent of zone-scale basal surfaces (dashed polygons).
341 Increasingly negative values (ms TWT) represent increasing depth below the sea floor, with 0 ms TWT at
342 sea level. The location of each zone is shown in Figure 2. A: Variance time slice of zone 1 at -308 ms TWT.
343 B: Interpretation of panel A showing 2 distinct long channelized features, and several short channelized
344 features. C: Time slice of zone 2 at -132 ms TWT. D: Interpretation of panel C showing 6 long channelized
345 features. E: Time slice of zone 2 at -192 ms TWT. F: Interpretation of panel E, showing many short

channelized features. G: Time slice of zone 3 at -220 ms TWT. H: Interpretation of panel H, showing 3 distinct long channelized features. I: Time slice of zone 3 at -280 ms TWT. J: Interpretation of panel I, showing several short channelized features. K: Time slice of zone 4 at -152 ms TWT. L: Interpretation of panel K, showing 6 distinct long channelized features and several short channelized features. The scalloped surface bounding the channelized features is mapped in a bold, solid black line.

Table 1 – Geometry of the short and long channelized features.

	channelized feature	
	short (n = 139)	**long (n = 17)**
length		
mean (m) ± standard error (m)	368 ± 16	5,251 ± 729
minimum (m)	95	1,644
maximum (m)	1,043	13,074
standard deviation (m) ± standard error (m)	188 ± 11	3,005 ± 531
feature-averaged width		
mean (m) ± standard error (m)	155 ± 4	250 ± 39
minimum (m)	72	140
maximum (m)	276	831
standard deviation (m) ± standard error (m)	48 ± 3	159 ± 28

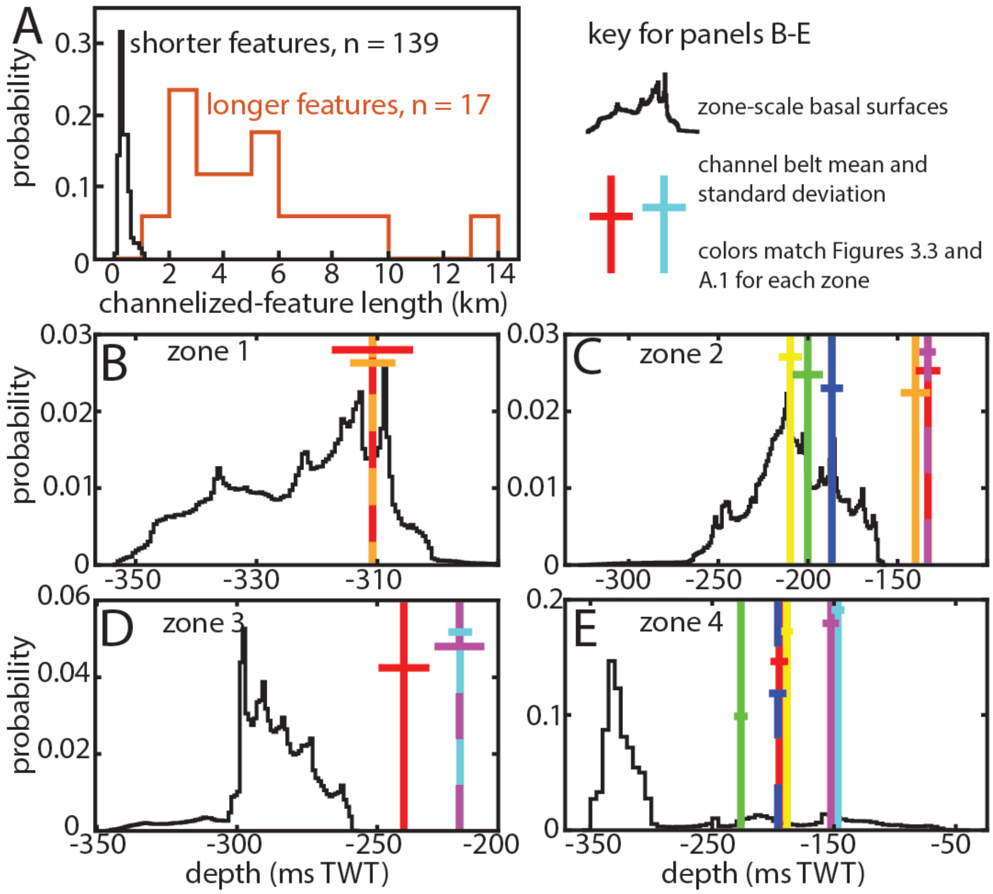

Figure 5 (9.1 cm x 8.2 cm) – A: Histogram comparing the two distinct channel belt populations based on their length normalized to their mean width. The black line represents the length distribution of shorter channelized features (red line) above which the longer channelized features (black line) sit. B-D: Black line histograms showing the distribution of depths for zone-scale basal surfaces in each zone. Depth is measured in milliseconds of two-way-travel time, which has a value of zero at sea level, with larger negative values representing greater depths into the subsurface. Colored vertical lines are placed at the mean depths of each well-preserved channel belt, with the standard deviation around the mean represented by the cross. The average stratigraphic position of a channel belt is within 10s of ms TWT above the basal surfaces. Line colors match belt colors in Fig. 4. E: Same as panels B-D, but the zone-scale basal surface of zone 4 is an incised valley (Fig. 4L), with the floor represented by the mode of the distribution, and the valley wall represented by the long, shallowing tail of the distribution.

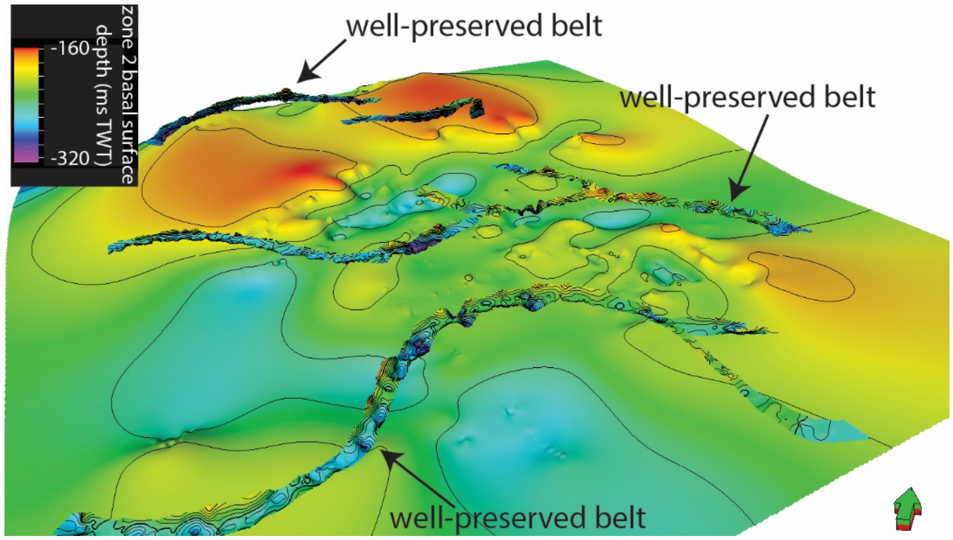

Figure 6 – Oblique view of the well-preserved channel belts and the zone 2 basal surface (Fig. 4C-F). The zone-scale basal surface is color-coded by depth (see legend) with a contour interval of 50 ms TWT. Depth contours for the mapped, overlying channel belts do not match each other or the zone-scale basal surface.

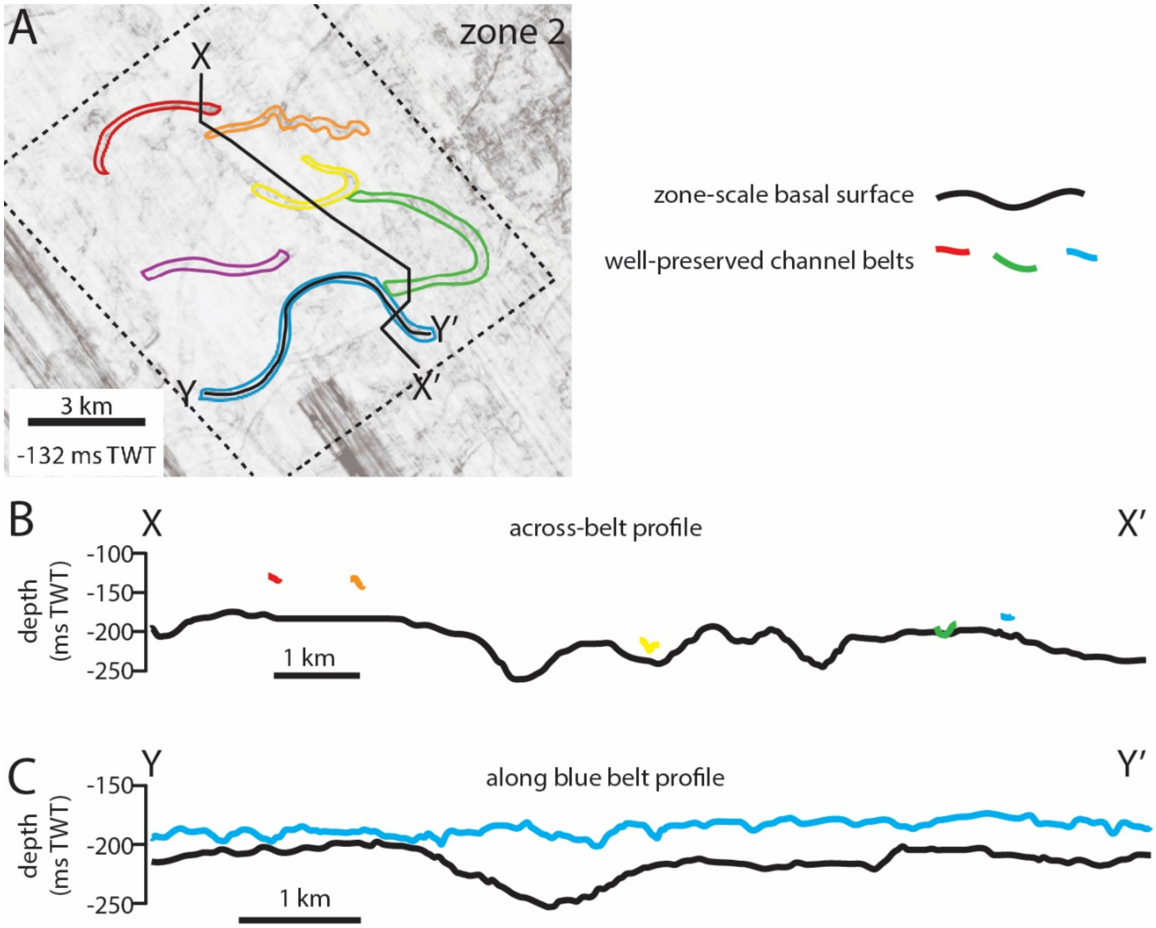

Figure 7 – A: Variance time slice of zone 2 at -132 ms TWT showing the 6 long channelized features. Two cross-sections are labeled. X-X′ runs roughly perpendicular to the channelized features, intersecting five of the six. Y-Y′ runs along the blue channelized feature. B: Depth profiles along transect X-X′ of the zone-scale basal surface (black line) and long channelized features (color lines, same colors as panel A). Belts sit less than 60 ms TWT above the zone-scale basal surface. Lateral distance is marked with a scale bar. C: Depth profile along transect Y-Y′, which follows the blue channelized feature. The blue channelized feature is consistently within 10 to a few 10s of ms TWT above the zone-scale basal surface.

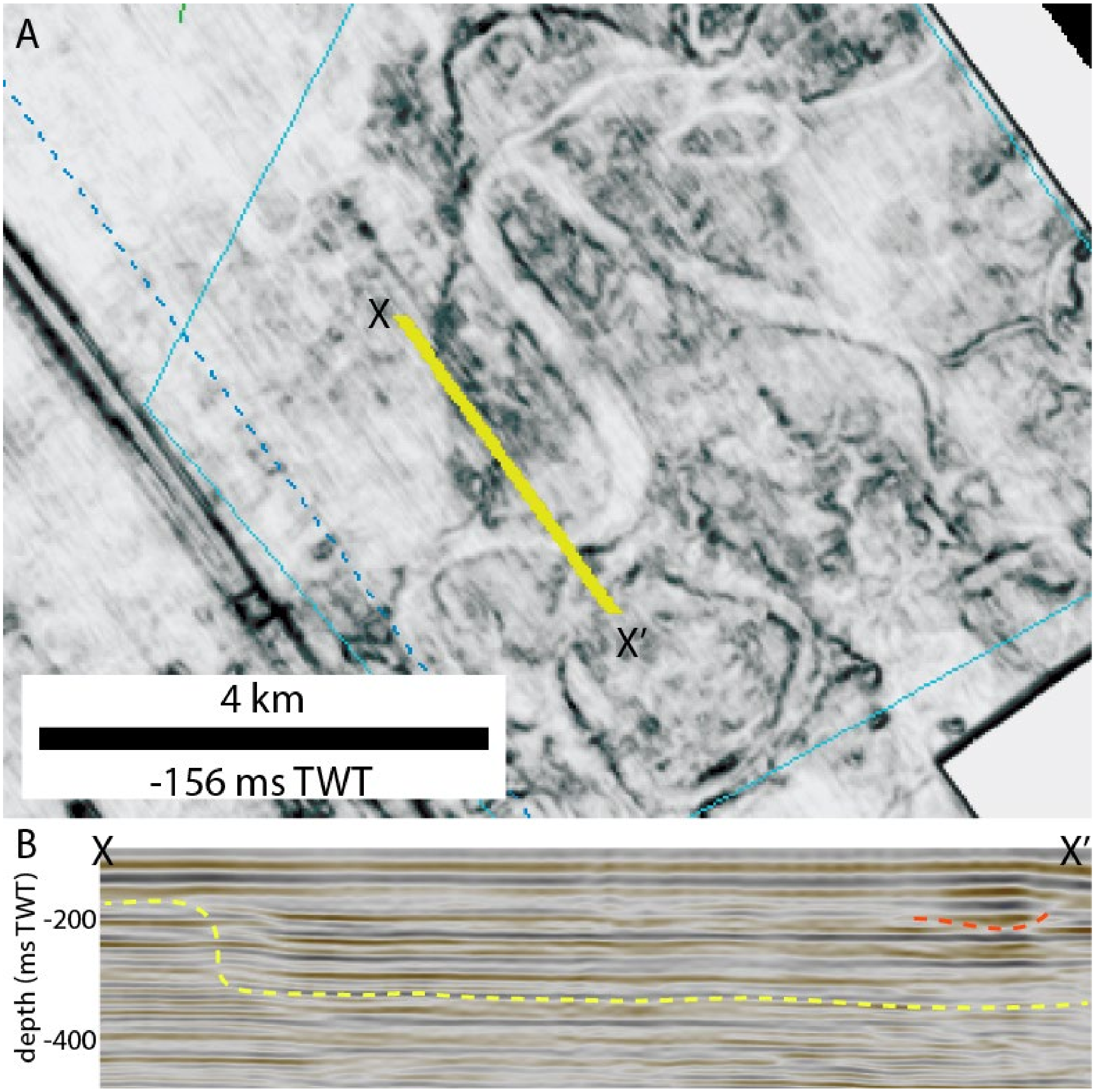

Figure 8 (18.5 cm x 18.4 cm) – A: Variance time slice of zone 4 showing cross-section X-X’, which cuts the valley wall. B: Cross-section X-X’, with a yellow dashed line marking the interpreted valley floor, wall, and outside the valley on the basis of reflectors changing from conformable, to truncated, to conformable, respectively. The red channel belt is shown within the valley as well (Fig. 4L).